Journal of
Applied and Computational Mechanics

Shahid Chamran
University of Ahvaz

Research Paper

Non-similar Radiative Bioconvection Nanofluid Flow under Oblique Magnetic Field with Entropy Generation

Nisha Shukla[1], Puneet Rana[2,3], S. Kuharat[4], O. Anwar Bég[4]

[1] Department of Mathematics, Institute of Applied Science and Humanities, GLA University, Mathura-281406, Uttar Pradesh, India

[2] School of Mathematical Sciences, College of Science and Technology, Wenzhou Kean University, Wenzhou 325060, China

[3] Department of Mathematics, Jaypee Institute of Information Technology, A-10, Sector 62, Noida 201309, India

[4] Aeronautical and Mechanical Engineering, University of Salford, Newton Building, M54WT, UK

Abstract. Motivated by exploring the near-wall transport phenomena involved in bioconvection fuel cells combined with electrically conducting nanofluids, in the present article, a detailed analytical treatment using homotopy analysis method (HAM) is presented of *non-similar bioconvection flow of a nanofluid under the influence of magnetic field (Lorentz force) and gyrotactic microorganisms*. The flow is induced by a stretching sheet under the action of an oblique magnetic field. In addition, nonlinear radiation effects are considered which are representative of solar flux in green fuel cells. A second thermodynamic law analysis has also been carried out for the present study to examine entropy generation (irreversibility) minimization. The influence of magnetic parameter, radiation parameter and bioconvection Rayleigh number on skin friction coefficient, Nusselt number, micro-organism flux and entropy generation number (EGN) is visualized graphically with detailed interpretation. Validation of the HAM solutions with published results is also included for the non-magnetic case in the absence of bioconvection and nanofluid effects. The computations show that the flow is decelerated with increasing magnetic body force parameter and bioconvection Rayleigh number whereas it is accelerated with stronger radiation parameter. EGN is boosted with increasing Reynolds number, radiation parameter and Prandtl number whereas it is reduced with increasing inclination of magnetic field.

Keywords: Non-similar; Bioconvection; Entropy; Oblique magnetic field; Homotopy Analysis Method.

1. Introduction

Solar energy is the one of the best source of renewable energy. The addition of solid nanoparticles in convective fluids can significantly enhance solar energy collection and heat transfer processes and has further benefits in terms of inexpensive implementation and sustainability. The suspension of nanoparticles in a base fluid is termed as "nanofluid" [1]–[5]. Hunt [6] was the first researcher who used deployed nanoparticles to collect solar energy. Shehzad *et al*. [7] have investigated a solar energy model for MHD three- dimensional flow of Jeffrey nanofluid. Das *et al*. [8] have extended this study and considered the nonlinear thermal radiation effect on mixed convection stagnation flow of nanofluid induced by a sheet with the effects of chemical reactions. Uddin *et al*. [9] have applied a FEM to investigate the multiple slips and nonlinear radiation effects on nanofluid flow. Khan *et al*. [10] have considered the thermal radiation effect on an electrically-conducting nanofluid flow over a moving wedge.

The study of Bioconvection flows arises due to up-swimming of microorganism (cause density variation) has significant importance in different regimes such as environmental systems, micro-channel/systems, fuel cells and biological polymer synthesis [11], [12]. Initially, Kuznetsov and Avramenko [13] have successfully studied the problem of bio-thermal stability utilizing nanofluids considering different boundary conditions. In 1992, the literature was successfully reviewed by Hill and Pedley [14] and later, Allouit *et al*. [15] has analyzed patterns in cylindrical domain to study the fluid momentum equation. The investigation of bioconvective fluid flow model induced by moving flat plate considering Stefan blowing effect is carried out by Uddin *et al*. [16]. The similar type of analysis on bioconvection involving Lie symmetries, slip flow, inclination of sheet, dual solution and stability analysis has been reported by Dhanai *et al*. [17]. Khan *et al*. [18] have applied RK7 shooting method to carried out the natural bioconvection nanofluid flow induced by a truncated cone. Waqas *et al*. [19] have investigated the influence of physical parameters on the second grade nanofluid flow induced by stretching surface with motile microorganism rate. They have observed that motile microorganism profile decreases with Prandtl number and Brownian motion parameter. Rashad *et al*. [20]have examined the bioconvection nanofluid flow with motile gyrotactic microorganisms over a horizontal circular cylinder using finite difference technique. The second law analysis of bioconvection MHD nanofluid flow examined by Khan *et al*. [21] between two stretchable rotating disk. They have applied the homotopy analysis method in this study. Recently, Aneja *et al*. [22] have investigated the effect of non-uniform magnetic field in the study of nanofluid flow containing the motile gyrotactic micro-organisms induced by a inclined nonlinear stretching sheet. They observed that as the thermophoresis parameter increases, the

rate of heat transfer decreases. Additionally, Khan *et al.* [23] have analyzed the Williamson nanofluid bioconvection flow through an oscillatory surface. Lu *et al.* [24] have investigated microorganism gyrotactic study on nanofluid flow in the neighborhood of stagnation point. They observed that microorganism distribution decreases for increasing the value of Peclet number.

The thermodynamic performance of any engineering system can be quantified by second law analysis which is based on the premise that the *entropy generation rate always increases in irreversible systems*. Viscous dissipation, Ohmic dissipation, rate of heat transfer and diffusion of nanoparticles are major sources which can generate entropy in electrically-conducting nanofluids. Entropy generation analysis has many applications in the optimization of industrial thermal devices and stores, geothermal energy systems, solar collector designs, heat transfer pipes, cooling of electronic devices *etc.* Singh *et al.* [25] have considered entropy generation in alumina-water nanofluids. Aïboud and Saouli [26] examined the entropy generation in viscoelastic fluid flow induced by stretching sheet. Butt *et al.* [27] studied entropy generation with thermal radiation and viscous dissipation effects in Blasius flow. Bhatti *et al.* [28] have analyzed the entropy generation for Eyring-Powell nanofluid flow over a stretching sheet. Bég *et al.* [29] presented the first solutions for magnetohydrodynamic swirling disk flow in hybrid nuclear propulsion with entropy generation, also plotting streamline and entropy distributions. Further studies of entropy generation minimization in energy and medical engineering sciences include Rashidi *et al.* [30] on hydromagnetic blood flows with lateral mass flux, Srinivas *et al.* [31] on radiative convection non-Newtonian channel flows, Akbar *et al.* [32] on biological cilia-generated propulsion of nanofluids with thermal convection and very recently Jangili and Bég [33] on hydromagnetic micropolar natural convection flows. Ramzan *et al.* [34] have studied the entropy generation for the carbon nanofluid bioconvection flow. Khan *et al.* [35] have investigated the effect of binary chemical reaction on entropy generation.

The important findings related to thermal transport in nanofluids including mathematical modeling (single/two phase), types and shape of nanoparticles, thermophysical properties and applications are discussed in reviews [36]–[42] and books [43]–[45]in detail. Further, Lyu *et al.* [46] have examined the experimental and theoretical study of MWCNT water nanofluid flow.

The present article, motivated by hybrid magnetohydrodynamic (MHD) bioconvection nanofluid fuel cells, considers the entropy generation analysis of non-similar MHD bioconvection flow of nanofluid over a stretching sheet (extending wall) with nonlinear solar radiation flux. In the literatures [47]–[51] authors have transformed the boundary layer PDE equations of nonsimilarity flow into ODE using nondimensional parameters and then applied homotopy analysis method (introduced by Liao [52])to solve these equations. Farooq *et al.* [53] have used the Mathematica package BVPH 2.0 to solve the nonsimilar boundary layer flow problem. In present article, we have successfully applied HAM to solve the dimensionless form of momentum, energy, nanoparticles mass and bioconvection (motile micro-organism species) equations which are the PDE with suitable boundary conditions. Extensive graphical and tabulated results are presented with validation where possible.

2. Mathematical Model

2D boundary layer incompressible MHD nanofluid flow with gyrotactic microorganisms is assumed through a stretching sheet. The swimming direction of microorganism is not affected by metallic nanoparticles. Heat transfer is considered along the sheet (horizontal axis) and solar flux is simulated with a *non-linear* thermal radiation model (Fig. 1).

A constant magnetic field B_0 is applied at inclination β to the sheet. Maxwell displacement and magnetic induction effects are neglected. According these assumptions, the mathematical model of present problem can be written as

$$\frac{\partial u_x}{\partial x} + \frac{\partial u_y}{\partial y} = 0. \tag{1}$$

$$\rho_{nf}\left(u_x \frac{\partial u_x}{\partial x} + u_y \frac{\partial u_x}{\partial y}\right) = \mu_{nf}\frac{\partial^2 u_x}{\partial y^2} + \left[(T-T_a)(1-C_a)\beta_1\rho_{nf} - (\rho_p - \rho_{nf})(C-C_a) - (N-N_a)(\rho_m - \rho_{nf})\gamma\right]g - \sigma_{nf}B_0^2\cos^2\beta\, u_x, \tag{2}$$
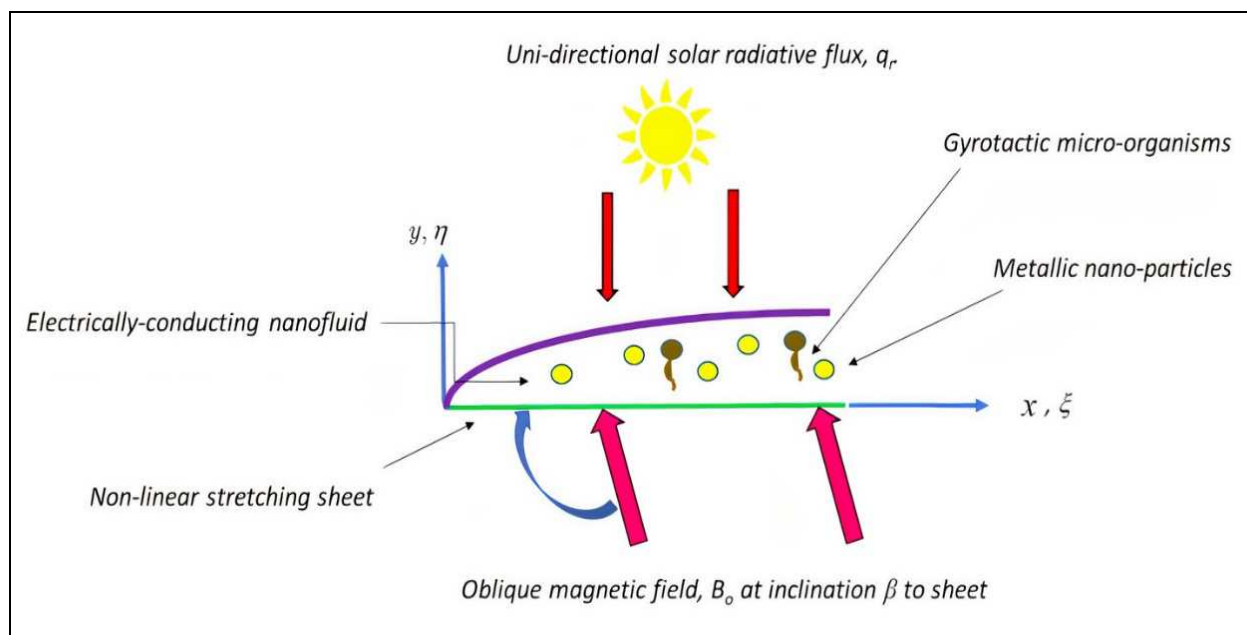

Fig. 1. Physical model for magnetic bioconvection nanofluid boundary layer flow under solar radiative flux.

$$(\rho c)_{nf}\left(u_x \frac{\partial T}{\partial x} + u_y \frac{\partial T}{\partial y}\right) = k_{nf}\frac{\partial^2 T}{\partial y^2} + D_B(\rho c)_p\left[\frac{\partial C}{\partial y}\frac{\partial T}{\partial y} + \frac{D_T}{D_B T_a}\left(\frac{\partial T}{\partial y}\right)^2\right] - \frac{\partial q_r}{\partial y},$$
(3)

$$u_x \frac{\partial C}{\partial x} + u_y \frac{\partial C}{\partial y} = D_B\left[\frac{\partial^2 C}{\partial y^2} + \frac{D_T}{D_B T_a}\frac{\partial^2 T}{\partial y^2}\right],$$
(4)

$$u_x \frac{\partial N}{\partial x} + u_y \frac{\partial N}{\partial y} + \frac{\partial}{\partial y}\left(N\frac{bW_c}{C_a}\frac{\partial C}{\partial y}\right) = D_m\frac{\partial^2 N}{\partial y^2},$$
(5)

restricted with the conditions

$$\text{at } y = 0, \qquad u_x = u_{xw}, \qquad u_y = 0, \quad T = T_w, \quad \frac{\partial C}{\partial y} + \frac{D_T}{D_B T_a}\frac{\partial T}{\partial y} = 0, \quad N = N_w$$

$$\text{as } y \to \infty, \qquad u_x = 0, \qquad T = T_a, \quad C = C_a, \quad N = N_a.$$
(6)

Here the Rosseland's approximation $q_r = -4\sigma_1/3k_1 \times \partial T^4/\partial y$ is used for radiative heat flux q_r. Apply transformations $x^* = x/l$, $y^* = y/l$, $u_x^* = u_x/u_{xw}$, $u_y^* = u_y/u_{xw}$, on eqs. (1)-(6), leading to:

$$\rho_{nf}\left(u_x^* \frac{\partial u_x^*}{\partial x^*} + u_y^* \frac{\partial u_x^*}{\partial y^*}\right) = \frac{\mu_{nf}}{u_{xw}l}\frac{\partial^2 u_x^*}{\partial y^{*2}} + \left[(1-C_a)(T-T_a)\beta\rho_{nf} - (\rho_p - \rho_{nf})(C-C_a) - (N-N_a)(\rho_m - \rho_{nf})\gamma\right]g - \sigma_{nf}B_0^2\cos^2\beta\frac{l}{u_{xw}}u_x^*,$$
(7)

$$(\rho c)_{nf}\left(u_x^* \frac{\partial T}{\partial x^*} + u_y^* \frac{\partial T}{\partial y^*}\right) = \frac{k_{nf}}{lu_w}\frac{\partial^2 T}{\partial y^{*2}} + \frac{D_B(\rho c)_p}{lu_{xw}}\left[\frac{\partial C}{\partial y^*}\frac{\partial T}{\partial y^*} + \frac{D_T}{D_B T_a}\left(\frac{\partial T}{\partial y^*}\right)^2\right] + \frac{16\sigma_1}{3k_1 lu_{xw}}\left[T^3\frac{\partial^2 T}{\partial y^{*2}} + 3T^2\left(\frac{\partial T}{\partial y^*}\right)^2\right],$$
(8)

$$u_x^* \frac{\partial C}{\partial x^*} + u_y^* \frac{\partial C}{\partial y^*} = D_B\left[\frac{1}{lu_{xw}}\frac{\partial^2 C}{\partial y^{*2}} + \frac{D_T}{D_B T_a lu_{xw}}\frac{\partial^2 T}{\partial y^{*2}}\right],$$
(9)

$$u_x^* \frac{\partial N}{\partial x^*} + u_y^* \frac{\partial N}{\partial y^*} + \frac{\partial}{lu_{xw}\partial y^*}\left(N\frac{bW_c}{C_a}\frac{\partial C}{\partial y^*}\right) = D_m\frac{\partial^2 N}{lu_{xw}\partial y^{*2}},$$
(10)

The transformed boundary conditions emerge as:

$$\text{at } y^* = 0, \qquad u_x^* = 1, \qquad u_y^* = 0, \quad T = T_w, \quad \frac{\partial C}{\partial y^*} + \frac{D_T}{D_B T_a}\frac{\partial T}{\partial y^*} = 0, \quad N = N_w,$$

$$\text{as } y^* \to \infty, \qquad u_x^* = 0, \qquad T = T_a, \quad C = C_a, \quad N = N_a.$$
(11)

we invoke the following relations and dimensionless parameters in eqs. (7)-(11):

$$u_x^* = \frac{\partial \psi^*}{\partial y^*}, \quad u_y^* = -\frac{\partial \psi^*}{\partial x^*}, \quad \theta^* = \frac{T-T_a}{T_w-T_a}, \quad \phi^* = \frac{C-C_a}{C_a}, \quad \chi^* = \frac{N-N_a}{N_w-N_a}, \quad Re = \frac{u_{xw}l}{v_{nf}}, \quad Pr = \frac{v_{nf}}{\alpha_{nf}}, \quad M = \frac{\sigma_{nf}B_0^2 l}{\rho_{nf}u_{xw}}, \quad Nb = \frac{(\rho c)_p}{(\rho c)_{nf}}\frac{D_B C_a}{\alpha_{nf}},$$

$$Nt = \frac{(\rho c)_p}{(\rho c)_{nf}}\frac{D_T(T_w-T_a)}{T_a \alpha_{nf}}, \quad Sc = \frac{v_{nf}}{D_B}, \quad R = \frac{4\sigma_1 T_a^3}{k_{nf}k_1}, \quad t_r = \frac{T_w}{T_a}, \quad Nr = \frac{(\rho_p - \rho_{nf})C_a}{\beta\rho_{nf}(1-C_a)(T_w-T_a)}, \quad Rb = \frac{(N_w-N_a)(\rho_m-\rho_{nf})\gamma}{\beta\rho_{nf}(1-C_a)(T_w-T_a)},$$

$$Ri = \frac{g(1-C_a)(T_w-T_a)\beta l}{u_{xw}^2}, \quad Pe = \frac{bW_c}{D_m}, \quad Sc_b = \frac{v_{nf}}{D_m}, \quad \Omega_\chi = \frac{N_a}{N_w-N_a}.$$
(12)

Next we introduce the scaling variables:

$$x^* = x', \ y^* = \frac{y'}{\sqrt{Re}}, \quad \psi^* = \frac{\psi}{\sqrt{Re}}, \quad \theta^* = \theta, \ \phi^* = \phi \text{ and } \chi^* = \chi.$$
(13)

After then, we apply the following non-similarity transformations on eqs. (9)-(11):

$$\eta = \frac{y'}{\sqrt{\xi}}, \quad \xi = x', \ \psi = f(\eta,\xi)\sqrt{\xi}, \quad \theta = \theta(\eta,\xi), \quad \phi = \phi(\eta,\xi), \quad \chi = \chi(\eta,\xi)$$
(14)

and obtained following dimensionless system of nonlinear partial differential equations

Momentum

$$\frac{\partial^3 f}{\partial \eta^3} + \frac{1}{2}f\frac{\partial^2 f}{\partial \eta^2} - M\cos^2\beta\xi\frac{\partial f}{\partial \eta} - \xi\left(\frac{\partial f}{\partial \eta}\frac{\partial^2 f}{\partial \xi\partial\eta} - \frac{\partial^2 f}{\partial \eta^2}\frac{\partial f}{\partial \xi}\right) + Ri\xi(\theta - Nr\phi - Rb\chi) = 0,$$
(15)

Energy

$$\frac{1}{\text{Pr}}\left(\frac{\partial^2\theta}{\partial\eta^2} + Nb\frac{\partial\theta}{\partial\eta}\frac{\partial\phi}{\partial\eta} + Nt\left(\frac{\partial\theta}{\partial\eta}\right)^2\right) + \frac{1}{2}f\frac{\partial\theta}{\partial\eta} - \xi\left(\frac{\partial f}{\partial\eta}\frac{\partial\theta}{\partial\xi} - \frac{\partial\theta}{\partial\eta}\frac{\partial f}{\partial\xi}\right) + \frac{4R}{3\text{Pr}}\left[(\theta(t_r-1)+1)^2\left((\theta(t_r-1)+1)\frac{\partial^2\theta}{\partial\eta^2} + 3(t_r-1)\left(\frac{\partial\theta}{\partial\eta}\right)^2\right)\right] = 0,$$ (16)

Nanoparticle Species

$$\frac{1}{\text{Sc}}\left(\frac{\partial^2\phi}{\partial\eta^2} + \frac{Nt}{Nb}\frac{\partial^2\theta}{\partial\eta^2}\right) + \frac{1}{2}f\frac{\partial\phi}{\partial\eta} - \xi\left(\frac{\partial f}{\partial\eta}\frac{\partial\phi}{\partial\xi} - \frac{\partial\phi}{\partial\eta}\frac{\partial f}{\partial\xi}\right) = 0,$$ (17)

Microorganism Species

$$\frac{\partial^2\chi}{\partial\eta^2} + Sc_b\left(\frac{1}{2}f\frac{\partial\chi}{\partial\eta} - \xi\left(\frac{\partial f}{\partial\eta}\frac{\partial\chi}{\partial\xi} - \frac{\partial\chi}{\partial\eta}\frac{\partial f}{\partial\xi}\right)\right) - Pe\left[(\chi+\Omega_\chi)\frac{\partial^2\phi}{\partial\eta^2} + \frac{\partial\chi}{\partial\eta}\frac{\partial\phi}{\partial\eta}\right] = 0,$$ (18)

Boundary Conditions

$$\text{at } \eta = 0, \qquad f = 0, \qquad \frac{\partial f}{\partial\eta} = 1, \qquad \theta = 1, \qquad \chi = 1, \qquad \frac{\partial\phi}{\partial\eta} + \frac{Nt}{Nb}\frac{\partial\theta}{\partial\eta} = 0,$$

$$\text{as } \eta \to \infty, \qquad \frac{\partial f}{\partial\eta} \to 0, \qquad \theta \to 0, \qquad \chi \to 0, \qquad \phi \to 0.$$ (1)

In fuel cell (solar) systems, key engineering design parameters include the sheet surface *shear stress (skin friction), the wall heat transfer gradient, wall nano-particle mass transfer gradient and wall motile micro-organism flux gradient* which can be written respectively as follows:

(i) Skin friction coefficient C_f

$C_f = \tau_w / \rho_{nf}u_{xw}^2$, where the shear stress τ_w is given as $\tau_w = \mu_{nf}\partial u_x / \partial y\big|_{y=0}$. Using the non-similarity transformations on C_f we obtain:

$$\sqrt{\text{Re}\,\xi}\ C_f = \frac{\partial^2 f}{\partial\eta^2}(0,\xi) = f''(0,\xi) = Cfr(\xi)$$ (20)

(ii) Local Nusselt number Nu

This defines the wall heat transfer gradient and also the ratio of convection to conduction heat transfer. It is given mathematically as follows:

$$Nu = \frac{l(q_w + q_r)}{k_{nf}(T_w - T_a)} .$$ (21)

Here

$$q_w = -k_{nf}\frac{\partial T}{\partial y}\bigg|_{y=0} - D_B h_p\rho_p\left(\frac{\partial C}{\partial y} + \frac{D_T}{D_B T_a}\frac{\partial T}{\partial y}\right)_{y=0} \quad \text{and} \quad q_r = -\frac{4\sigma_1}{3k_1}\frac{\partial T^4}{\partial y}, \quad h_p = c_p T .$$ (22)

Using eq. (20) and the definitions of q_w and q_r in Nu then we obtain:

$$\sqrt{\frac{\xi}{\text{Re}}}Nu = -\frac{\partial\theta}{\partial\eta}(0,\xi)\left[1 + \frac{4R}{3}t_r^3\right] = -\theta'(0,\xi)\left[1 + \frac{4R}{3}t_r^3\right] = Nur(\xi).$$ (23)

(iii) Local Sherwood number Sh

This defines the wall mass transfer gradient for nano-particle species, and takes the form:

$$Sh = \frac{lq_m}{D_B(C_w - C_a)}.$$ (24)

Here *wall nano-particle mass flux* is given by:

$$q_m = \frac{j_p}{\rho_p} = \left(\frac{\partial C}{\partial y} + \frac{D_T}{D_B T_a}\frac{\partial T}{\partial y}\right)_{y=0} = 0.$$ (25)

Hence Sherwood number is zero.

(iv) Local wall motile microorganism flux Nn

Micro-organism species gradient at the wall (sheet) is quantified by *Nn* which is defined as:

$$Nn = \frac{lq_n}{D_m(N_w - N_a)}. \tag{26}$$

Here the *wall motile microorganism flux* q_n is given by:

$$q_n = -D_m\left(\frac{\partial N}{\partial y}\right)_{y=0}. \tag{27}$$

Using eq. (20) we arrive at

$$\sqrt{\frac{\xi}{\text{Re}}}Nn = -\frac{\partial \chi}{\partial \eta}(0,\xi) = -\chi'(0,\xi) = Nnr(\xi). \tag{28}$$

3. Second Law Thermodynamic Analysis

Bejan [54] has derived the expression of volumetric rate of entropy generation S_G. For the present problem S_G is defined as:

$$S_G = \frac{k_{nf}}{T_a^2}\left[1 + \frac{16\sigma_1 T_a^3}{3k_{nf}k_1}\right]\left(\frac{\partial T}{\partial y}\right)^2 + \frac{1}{T_a}\left[\mu_{nf}\left(\frac{\partial u_x}{\partial y}\right)^2\right] + \frac{\sigma_{nf}B_0^2\cos^2\alpha}{T_a}u_x^2 + \frac{R_g D_B}{C_a}\left(\frac{\partial C}{\partial y}\right)^2 + \frac{R_g D_B}{T_a}\left(\frac{\partial T}{\partial y}\right)\left(\frac{\partial C}{\partial y}\right) = S_t + S_v + S_o + S_d \tag{29}$$

In eq. (29), $S_t = k_{nf}/T_a^2 \times [1 + (16\sigma_1 T_a^3)/(3k_{nf}k_1)](\partial T/\partial y)^2$, $S_v = 1/T_a \times [\mu_{nf}(\partial u_x/\partial y)^2]$, $S_o = \sigma_{nf}B_0^2 u_x^2 \cos^2\alpha/T_a$ and $S_d = R_g D_B/C_a(\partial C/\partial y)^2$ $+ R_g D_B/T_a(\partial T/\partial y)(\partial C/\partial y)$ are the entropy generation (EG) generated by heat transfer, viscous dissipation, Ohmic dissipation and nanoparticles diffusion, respectively.

The characteristic entropy S_C is defined as:

$$S_C = \frac{k_{nf}(T_w - T_a)^2}{l^2 T_a^2}. \tag{30}$$

Apply the non-similarity transformations defined in Eq. (14) to the ratio of S_G to S_C then we obtain:

$$N_S = \frac{\text{Re}}{\xi}\left[\left(1 + \frac{4R}{3}\right)\theta'^2 + \frac{\text{Pr.Ec}}{\Omega}\left\{f''^2 + \xi M\cos^2\alpha f'^2\right\} + \frac{\chi_e}{\Omega}\left(\frac{1}{\Omega}\phi'^2 + \theta'\phi'\right)\right], \tag{31}$$

where $\chi_e = RD_B C_a/k_{nf}$ and $\Omega = (T_w - T_a)/T_a$.

4. Homotopy Analysis Method

Although many semi-analytical and numerical methods are available for solving nonlinear coupled systems of partial differential equations, here we implement the excellent homotopy analysis method (HAM). The definitive treatise on this approach is given by Liao [52]. The technique has been implemented in an extensive range of fluid dynamics applications in the past decade. These include bio-rheological smart magnetic lubrication analysis [55], coating of industrial components with nanofluids [56], biophysical propulsion [57], mixing processes in chemical engineering [58], biological surface coating physics [59]. Very recently Bég [60] has provided an extensive review of HAM applications in nonlinear electromagnetic pumping flows. Further applications are provided in Abdallah [61] (on magneto-convection), Hayat et al. [62] (on slip Sakiadis flows), Liao [63] (on variations of HAM), Gupta and Gupta [64] (on nonlinear Cauchy problems), Van Gorder *et al.* [65] (on convergence aspects of HAM) and Yin *et al.* [66] (on fractional wave equations). Applying HAM to Eqns. (15)-(18), we define the following initial guesses, linear operators and auxiliary parameter:

$$f_0(\eta,\xi) = 1 - e^{-\eta}, \quad \theta_0(\eta,\xi) = e^{-\eta}, \quad \phi_0(\eta,\xi) = -\frac{Nt}{Nb}e^{-\eta}, \quad \chi_0(\eta,\xi) = e^{-\eta}. \tag{32}$$

$$L_f = \frac{\partial^3 f(\eta,\xi)}{\partial \eta^3} - \frac{\partial f(\eta,\xi)}{\partial \eta}, \quad L_\Omega = \frac{\partial^2 \Omega(\eta,\xi)}{\partial \eta^2} + \frac{\partial \Omega(\eta,\xi)}{\partial \eta}, \quad \text{where} \quad \Omega = \theta,\phi \quad \text{and} \quad \chi. \tag{33}$$

The mth order deformation equations are defined as:

$$L_\Theta[\Theta_m(\eta,\xi) - \Psi_{m-1}\Theta_{m-1}(\eta,\xi)] = h_\Theta H_\Theta R_m^\Theta(\eta,\xi), \text{ and } H_\Theta = 1, \tag{34}$$

where $\Theta = f, \theta, \phi$ and χ with boundary conditions

$$\text{at } \eta = 0, \quad f_m = 0, \quad \frac{\partial f_m}{\partial \eta} = 0, \quad \theta_m = 0, \quad \frac{\partial \phi_m}{\partial \eta} + \frac{Nt}{Nb}\frac{\partial \theta_m}{\partial \eta} = 0, \quad \chi_m = 0,$$

$$\text{as } \eta \to \infty, \quad \frac{\partial f_m}{\partial \eta} \to 0, \quad \theta \to 0, \quad \phi_m \to 0, \quad \chi_m \to 0. \tag{35}$$

Here the functions $R_m^f(\eta,\xi)$ are defined as

$$R_m^{\Theta}(\eta,\xi) = \frac{1}{m-1!}\frac{\partial^{m-1}N_{\Theta}}{\partial q^{m-1}}\bigg|_{q=0},$$

(36)

where $\Theta = f, \theta, \phi$ and χ are obtained from eqs. (15)-(18). The function $\Psi_m = 0$ for $m \leq 1$ and $\Psi_m = 1$ for $m > 1$. The convergence is dependent upon the parameters h_f, h_{θ}, h_{ϕ} and h_{χ}. The solutions $f(\eta,\xi)$, $\theta(\eta,\xi)$, $\phi(\eta,\xi)$ and $\chi(\eta,\xi)$ are generated thereby as the following power series expansions:

$$\Phi(\eta,\xi) = \Phi_0(\eta,\xi) + \sum_{m=1}^{\infty}\Phi_m(\eta,\xi),$$

(37)

where $\Phi = f, \theta, \phi$ and χ.

4.1. Convergence of HAM

To determine suitable values of the auxiliary parameters h_f, h_{θ}, h_{ϕ} and h_{χ} we have plotted h-curves with $f''(0,\xi)$, $\theta'(0,\xi)$, $\phi'(0,\xi)$ and $\chi'(0,\xi)$ for different values of the non-similar parameter ξ which are shown in Fig. 2. In Fig. 2, horizontal lines are obtained in the ranges $h_f = [-0.65, -0.3]$, $h_{\theta} = [-0.5 -0.005]$, $h_{\phi} = [-0.5 -0.005]$, $h_{\chi} = [-0.6 -0.025]$. It has been observed that the values of $f''(0,\xi)$, $\theta'(0,\xi)$, $\phi'(0,\xi)$ and $\chi'(0,\xi)$ are convergent up to four decimal places for $h_f = -0.4$, $h_{\theta} = -0.3$, $h_{\phi} = -0.3$, $h_{\chi} = -0.3$. These values are shown in Table-1. The residual errors E_f, E_{θ}, E_{ϕ} and E_{χ} for the velocity, temperature, concentration and microorganism respectively are defined as

$$E_{\Phi} = \frac{1}{LK}\sum_{i=1}^{L}\sum_{j=1}^{K}\left[N_{\Phi}\left(\sum_{n=0}^{m}\Phi_n(\eta,\xi)\right)_{(\eta=i(\delta\eta),\,\xi=j(\delta\xi))}\right]^2$$

(38)

where $\Phi = f, \theta, \phi$ and χ, and $\delta\eta$, $\delta\xi$ are step lengths (increment) and LK corresponds to total number of data. The 2500 data set are compared and residual errors are displaced in Table-2 for different order of approximations, m which shows that error decreases with increment in the value of m. Thus, it gives us confidence that selected value of auxiliary parameters led us to get convergent solution with desired accuracy for $m = 12$.

5. Computational Results and Discussion

The HAM solutions have been evaluated numerically with MAPLE symbolic software. in Figs. 3-8. These figures allow a parametric analysis of the influence of magnetic parameter M, radiation parameter R and Prandtl number Pr on temperature, skin friction, Nusselt number and rate of motile microorganism density at the surface and entropy generation number, values of involving parameters are fixed as:

$Pr = 5$, $M = 1$, $Nb = Nt = Nr = 0.1$, $Ri = 0.5$, $Sc_b = 1$, $Sc = 2$, $\beta = \frac{\pi}{4}$, $Pe = 1$, $\Omega_{\chi} = 0.1$, $Rb = R = 0.1$, $tr = 0.5$, $\chi_e = 0.005$, $\Omega = 0.1$.
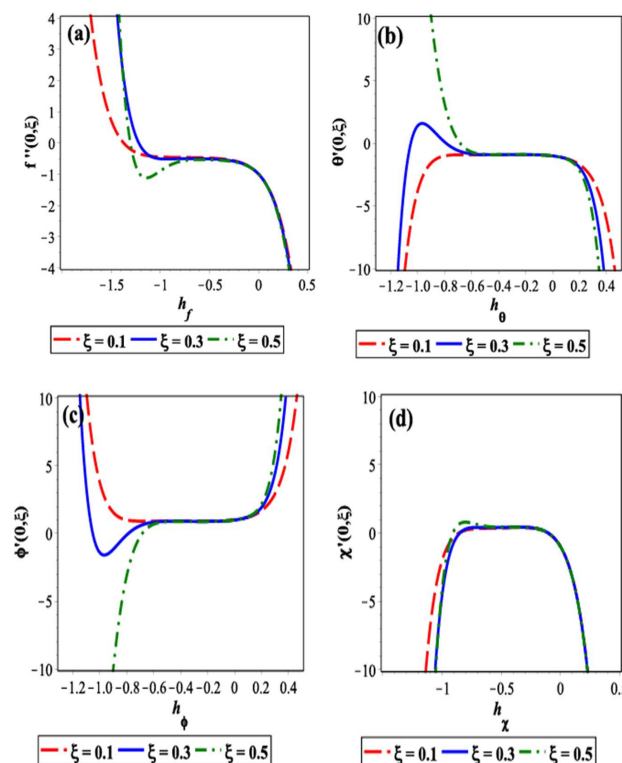

Fig. 2. *h-ranges* of h_f, h_{θ}, h_{ϕ} and h_{χ} for different values of ξ.

Table 1. Order of Convergence: $Pr = 1$, $M = 0.1$, $Nb = Nt = 0.1$, $Sc = 2$, $\beta = \pi / 4$, $Ri = 3$, $Scb = 1$, $Pe = 1$, $\Omega_\chi = 0.1$, $Rb = R = 0.1$, $Nr = 0.1$, $tr = 0.1$, $\xi = 0.1$.

Order of approximation	$\{-f''(0,\xi)\}$	$\{-\theta'(0,\xi)\}$	$\phi'(0,\xi)$	$-\chi'(0,\xi)$
5	-0.3915	0.4658	0.4110	-0.0401
9	-0.2975	0.4724	0.4168	-0.1096
12	-0.2767	0.4802	0.4237	-0.1242
15	-0.2697	0.4812	0.4246	-0.1265
20	-0.2687	0.4811	0.4246	-0.1264

Table 2. Convergence of HAM via squared residual error

$Pr = 1$, $M = 0.1$, $Nb = Nt = 0.1$, $Sc = 2$, $\beta = \pi / 4$, $Ri = 3$, $Scb = 1$, $Pe = 1$, $\Omega_\chi = 0.1$, $Rb = R = 0.1$, $Nr = 0.1$, $tr = 0.1$, $\xi = 0.1$.

Order of approximation	E_f	E_θ	E_ϕ	E_χ
2	1.1342×10^{-1}	4.5899×10^{-2}	3.3387×10^{-2}	5.6566×10^{-2}
4	9.7085×10^{-3}	8.7869×10^{-3}	2.7893×10^{-2}	2.6946×10^{-2}
6	2.6726×10^{-3}	4.5972×10^{-4}	2.2762×10^{-2}	1.0217×10^{-2}
8	1.3005×10^{-3}	3.9521×10^{-4}	1.9032×10^{-2}	3.5005×10^{-3}
10	3.7030×10^{-4}	2.0927×10^{-4}	7.6156×10^{-3}	1.6960×10^{-3}
12	7.4016×10^{-5}	8.3083×10^{-5}	1.7122×10^{-4}	8.9124×10^{-4}

Table 3. Comparison of Present Results with Previous Published Results, $M = Nt = Nb = 0$, $\xi = 0$.

Pr	Present	Dhanai et al. [17]	Wang [54]	Khan and Pop [55]	Gorla and Sidawi [56]
0.2	0.1691	0.1692	0.1691	0.1691	0.1691
0.7	0.4539	0.4539	0.4539	0.4539	0.5348
2	0.9114	0.9113	0.9114	0.9113	0.9114
7	1.8954	1.8954	1.8954	1.8954	1.8904

Table 4. Present values of skin friction coefficient *Cfr,* Nusselt number *Nur,* wall motile microorganism flux *Nnr* with variation of ξ and fixed values of other parameters for twelth order of convergence.

	Rb = 0.1			Rb = 0.2			Rb = 0.3		
ξ	Cfr	Nur	Nnr	Cfr	Nur	Nnr	Cfr	Nur	Nnr
0.1	-0.4450	1.1801	0.4950	-0.4502	1.1784	0.4970	-0.4554	1.1768	0.4990
0.2	-0.4330	1.1812	0.4971	-0.4434	1.1779	0.5010	-0.4538	1.1746	0.5050
0.3	-0.4210	1.1824	0.4991	-0.4364	1.1775	0.5048	-0.4521	1.1724	0.5108
0.4	-0.4089	1.1836	0.5009	-0.4294	1.1771	0.5084	-0.4503	1.1702	0.5164
0.5	-0.3969	1.1851	0.5025	-0.4224	1.1768	0.5117	-0.4484	1.1681	0.5217

Table 5. Effect of the thermophoresis parameter *Nt*, nonlinear radiation parameter *R*, magnetic parameter *M* and Rayleigh number *Rb* on the Nusselt number for the fixed values of others parameters with twelth order of convergence.

		(M,Rb)		
Nt	R	(0.1,0.1)	(0.2,0.1)	(0.1,0.2)
	0.1	0.4802	0.4795	0.4753
0.1	0.2	0.4968	0.4979	0.4941
	0.3	0.5174	0.5166	0.5134
0.2	0.1	0.4689	0.4681	0.4617
0.3		0.4571	0.4563	0.4467

We have compared the values of rate of heat transfer $\{-\theta'(0,\xi)\}$ with the previous published values in the absence of magnetic field, nanoparticles and bioconvection in Table-3**.** This comparison is performed for self-similar flow in the absence of magnetic field (*i.e.* electrically *non-conducting* nanofluids) and evidently very good agreement with Wang [67], Khan and Pop [68] and Gorla and Sidawi [69].

It is noticed from Table-4 that the values of skin friction coefficient are decreased with an increase in the value of ξ whereas the rate of heat transfer (Nusselt number) and motile organism flux are increased with this parameter. The present HAM values of Nusselt number with variation of thermophoresis parameter *Nt,* nonlinear radiation parameter *R,* magnetic parameter and Rayleigh number *Rb* are tabulated in Table-5. This table shows that the nonlinear parameter is the key factor to increase the rate of heat transfer at the surface. Consequently, other parameters are retarding parameters for the local Nusselt number.

Fig. 3 is plotted to check the behavior of streamlines (Contour ranges: 0.1820 to 1.3821) and isotherms (Contour ranges: 0.8633 to 0.0770). It can be easily seen that momentum boundary layer (impact reaches y*>1) is higher than thermal boundary layer. The influence of several parameters is also shown on Nusselt number (Fig.4). The micro-organism parameters, Pe and Ω has same and diminishing effect on Nusselt number and Prandtl number (*Pr*) has significant influence as compared to Nt on Nur. The value of $Ri \approx 3.5$ without microorganism has maximum heat transfer for default set of parameters. Increment in Rb enhances temperature in boundary layer thus causes decrement in Nusselt number (shown in. Fig. 4(c)).
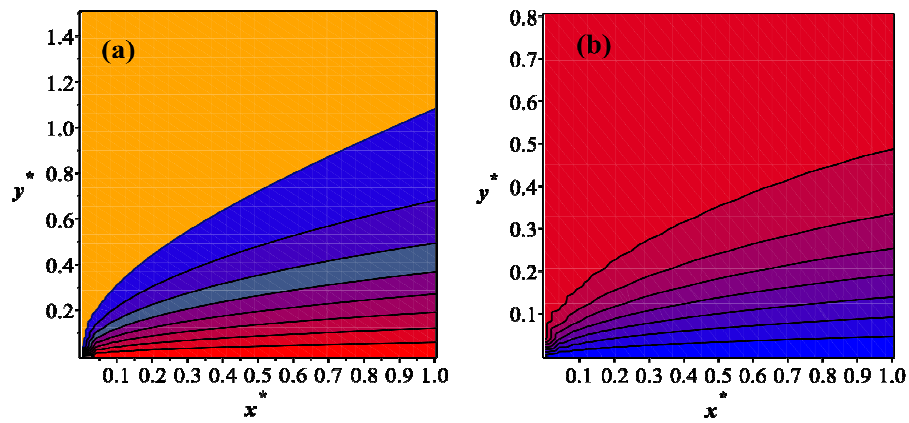
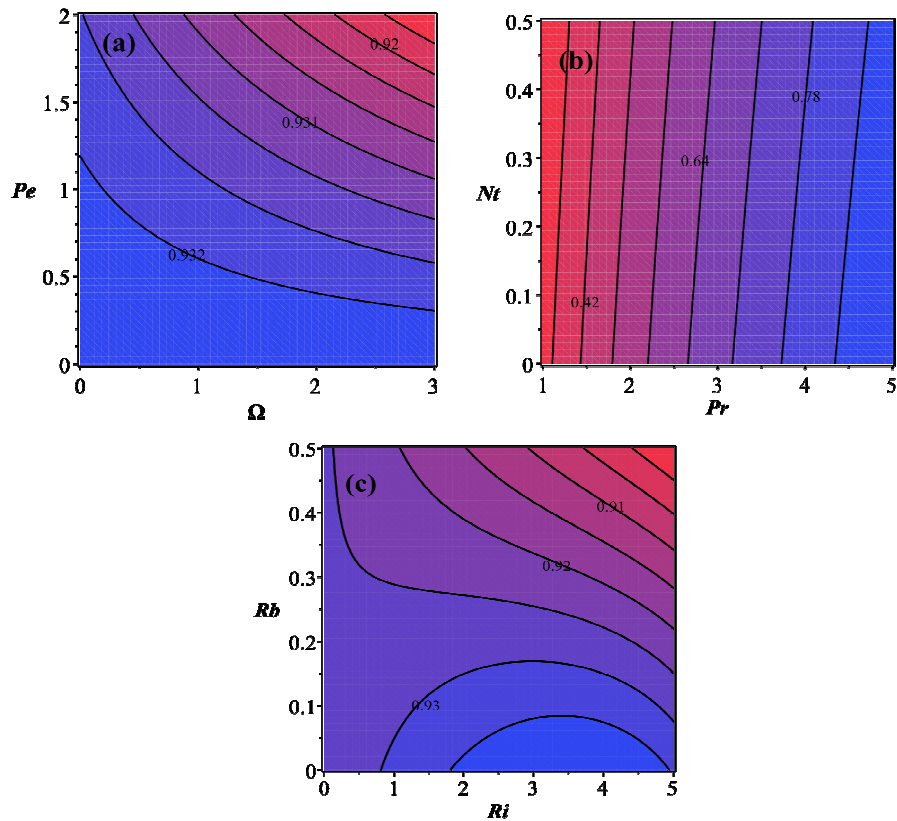**Fig. 3.** Representation of streamlines (left) and isotherms (right).

Fig. 4. Influence of various parameters (a) Micro-organism (Pe, Ω) (b) (Nt, Pr) (c) Buoyancy parameter (Rb, Ri) on Nusselt number.
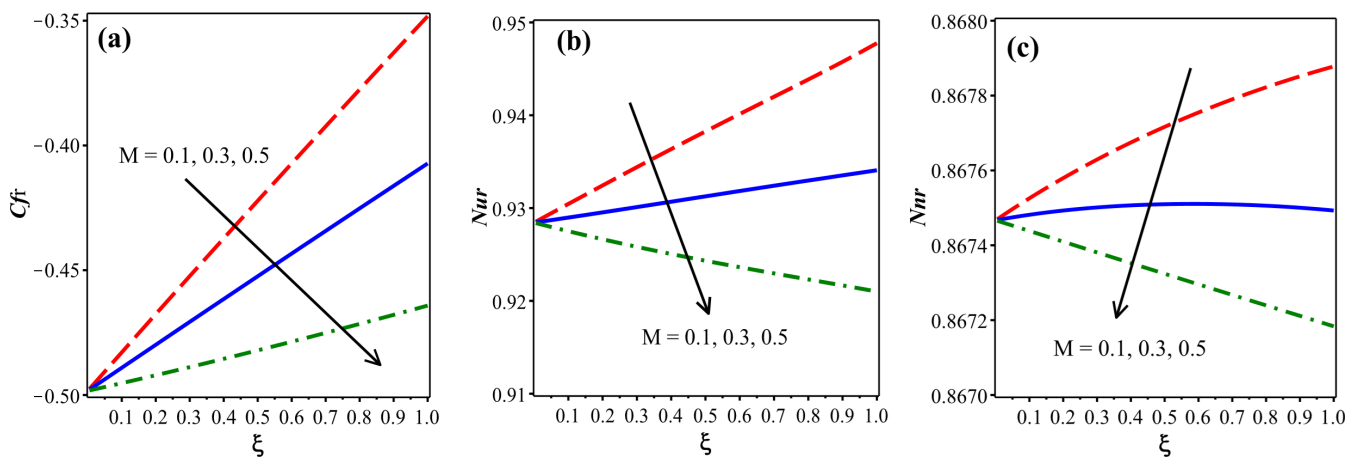

Fig. 5. Influence of magnetic parameter (M, ξ) on skin friction, Nusselt number and motile microorganism flux.

Fig. 5 and Fig. 6 are examined the influence of magnetic and non-similar (streamwise coordinate), parameters on skin friction coefficient (*Cfr*), Nusselt number (*Nur*) and motile microorganism density number gradient (*Nnr*), respectively. Fig. 5 shows that that Nusselt number, skin friction and motile microorganism flux are all decreasing functions of magnetic parameter, *M*. The magnetic body force term generates impedance to the flow which induces deceleration throughout the boundary layer. This effectively decreases the shearing stress at the wall and suppresses skin friction (*Cfr*). The magnetic field therefore clearly has an inhibiting effect on the flow and enhances momentum boundary layer thickness. The additional work which must be expended to drag the nanofluid against the action of the magnetic field (the oblique orientation is considered, nevertheless there is still a transverse component which manifests as the Lorentz body force) is dissipated as thermal energy (heat) within the body of the nanofluid. This causes heat to be drawn away from the wall also and results in a decrease in heat transfer rate to the wall i.e. a reduction in Nusselt number (*Nur*). Simultaneously the thermal boundary layer thickness is enhanced. These trends concur with numerous other studies in the literature including the classical work of Cramer *et al.* [70] and more recently for nanofluid magnetic bioconvection in the work of Dhanai *et al.* [17]. The opposition to momentum development and the retardation in the flow encourages the diffusion of micro-organisms within the boundary layer and the migration of this species away from the wall, as noted in Uddin *et al.* [16], [71]. This decreases the rate of motile micro-organism diffusion to the wall (sheet) and the upshot is therefore depletion in motile microorganism flux (*Nnr*). Overall therefore the significant influence of magnetic field on transport characteristics is confirmed with our results and the deployment of magnetized bioconvection nanofluids in fuel cells would appear to be a promising venture for energy resources technologies, as further corroborated in Katz *et al.* [72] and Goh *et al.* [73].

In Fig. 6, an increase in radiation parameter is observed to substantially enhanced skin friction (*Cfr*) and motile microorganism flux (*Nnr*) whereas it significantly reduces the Nusselt number (*Nur*). The Rosseland approximation which has been used to simulate radiative solar flux is valid for *optically-thick nanofluids* which can absorb or emit radiation at their boundaries. The energization of the magnetic nanofluid results in the progressive removal of heat from the wall (sheet) which decreases Nusselt number magnitudes. However, the acceleration in the boundary layer flow results in a boost in skin friction at the wall. Although radiative flux does not feature in either the momentum or micro-organisms species conservation equations, via the thermal modification in the flow, both velocity and micro-organism density number fields are significantly altered. The acceleration in the flow aids in the diffusion of micro-organisms towards the wall which manifests in an elevation in motile microorganism flux (*Nnr*). Solar radiative flux therefore is observed to work quite well in conjunction with nanofluid species and micro-organism species diffusion and this would suggest that hybrid nano-bio-fuel cells holds some promise in renewable energy systems.

From Fig. 7, it can be observed that *Cfr* , *Nur* and *Nnr* are all decreased with increment in the value of bioconvection Rayleigh number *Rb*. The bioconvection Rayleigh number $Rb = [(N_w - N_\infty)(\rho_m - \rho_{nf})\gamma] / [\beta\rho_{nf}(1 - C_\infty)(T_w - T_\infty)]$ features in the momentum equation (15) in the term $-Ri\xi Rb\chi$ and effectively couples the momentum (velocity) field with the micro-organism number density field. The dominant effect of increasing *Rb* is to decelerate the magnetic nanofluid boundary layer and to effectively reduce the momentum (velocity) boundary layer thickness. Skin friction is therefore also reduced since the nanofluid shears slower past the stretching wall. The reduction in skin friction however serves to enhance the diffusion into the boundary layer of nano-particles and micro-organisms. The rate of transfer of nanoparticles and micro-organisms to the wall is therefore stifled and this will manifest in a plummet in both Nusselt number (*Nur*) and motile microorganism flux (*Nnr*), as visualized in Fig. 7 b, c, respectively.

Fig. 8 is plotted to express the impact of radiation parameter *R* and Prandtl number on temperature. It indicates that the increasing value of radiation parameter improves the temperature of nanofluid whereas higher Prandtl number induces the opposite behavior. As noted earlier greater solar radiative flux energizes the nanofluid which elevates temperatures (and reduced Nusselt numbers). The Prandtl number (*Pr*) is prescribed values higher than unity which are appropriate for highly-doped water-based magnetic nano-particle suspensions. For Prandtl number of unity, both the boundary layers (momentum and temperature) are of the same thickness. However, when Prandtl number exceeds unity, the thickness of temperature boundary layer is less than the momentum boundary layer thickness. Generally, higher *Pr* fluids lower nanofluid temperatures in the boundary layer regime which is undesirable in solar nano-materials.
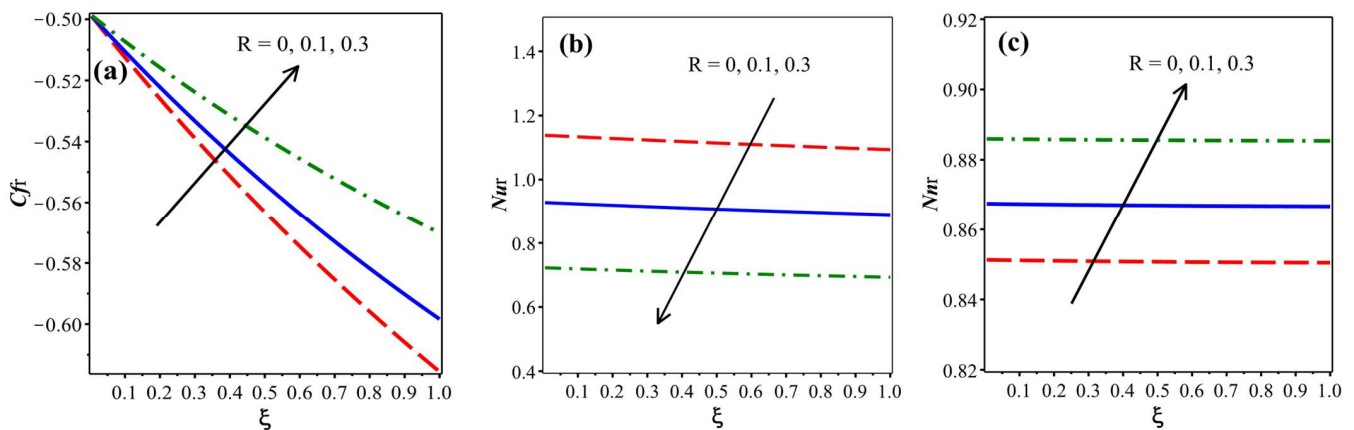

Fig. 6. Effect of radiation parameter *R* on skin friction, Nusselt number and motile microorganism flux.
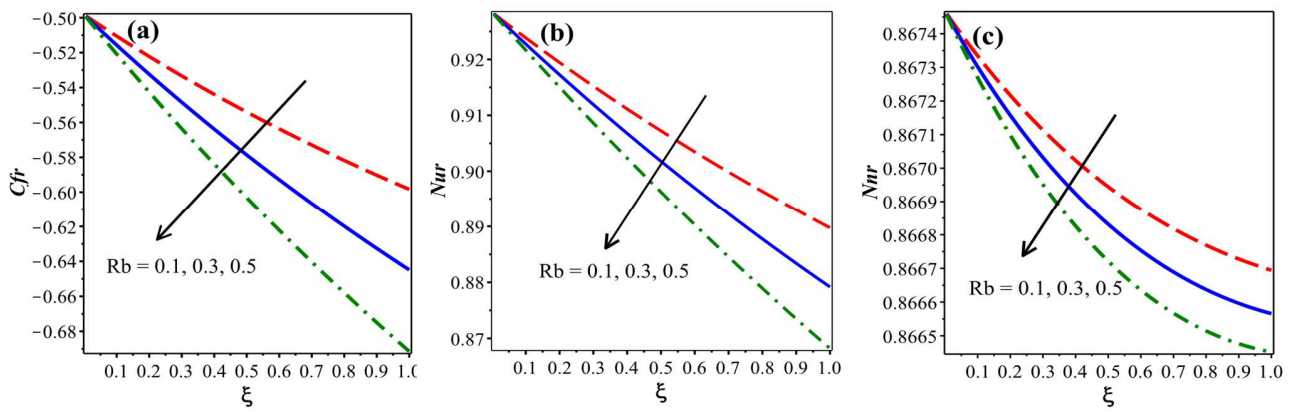
Fig. 7. Effect of bioconvection Rayleigh number on skin friction, Nusselt number and motile organism flux.
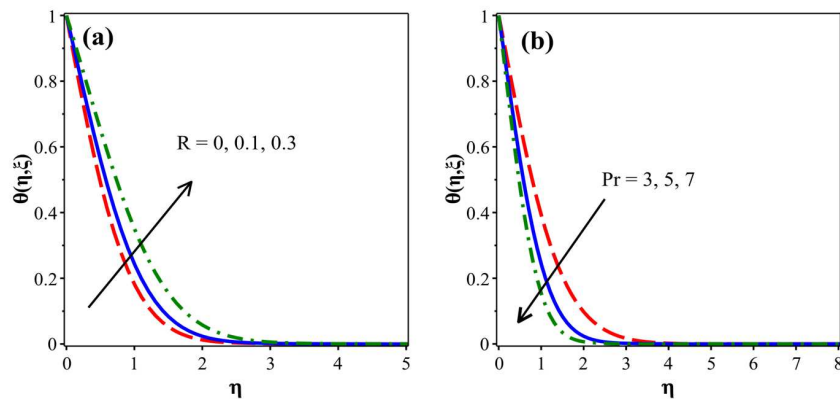

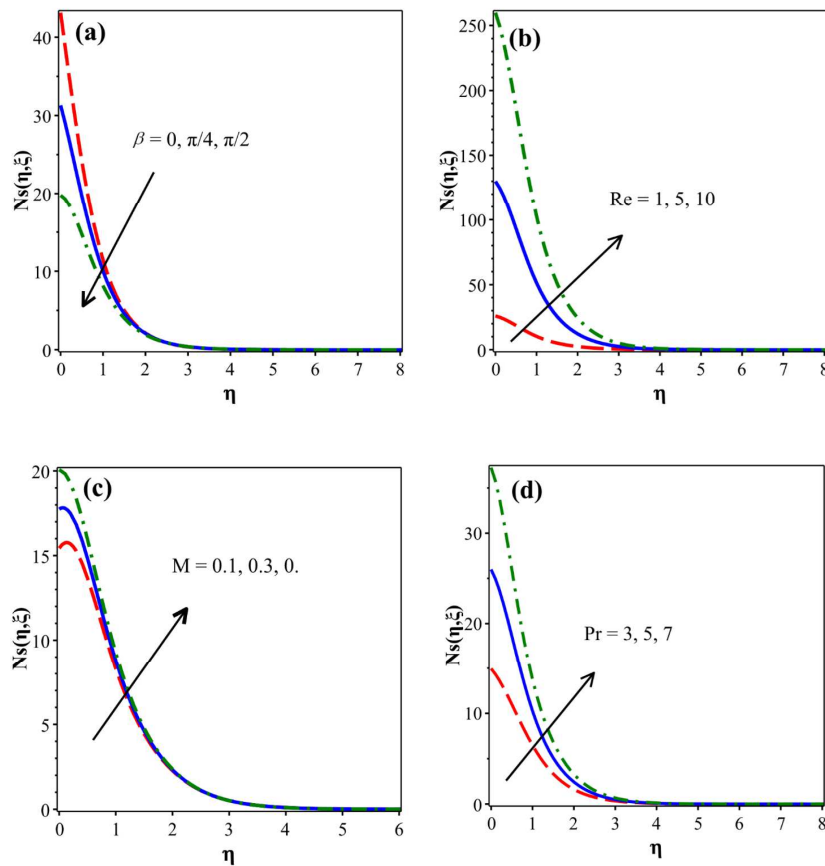**Fig. 8.** Effect of radiation parameter and Prandtl number on temperature.

Fig. 9. Effect of β, Re, M and Pr on entropy generation number.

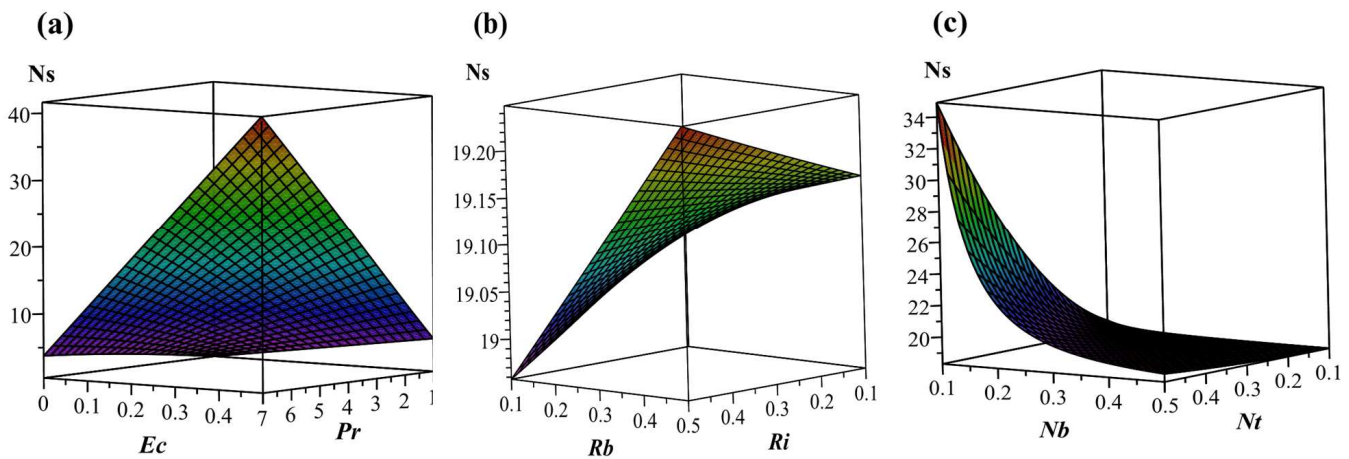**(a)**   **(b)**   **(c)**

Fig. 10. Combined impact of (Pr, Ec), (Ri, Rb) and on entropy generation number.

Fig. 9 depicts the influence of magnetic field inclination (β), Reynolds number (Re), magnetic parameter (M) and Prandtl number (Pr) on entropy generation number. This figure illustrates that Re, M and Pr are responsible for enhancing the entropy generation in the system whereas greater inclination of magnetic field generates a reduction in entropy generation (the magnetic body force is reduced with increasing values of inclination angle and is a maximum only for the zero inclination case, for which cosine function attains a maximum value of unity). A combined influence of physical parameters on entropy generation number is shown in Fig. 10, which represents that Ns is an increasing function of several controlling parameters such as Prandtl number, Eckert number, mixed convection parameter, Rayleigh number Rb and thermophoresis parameter whereas it decreases with an enhancement in the value of Brownian motion parameter.

6. Concluding Remarks

A mathematical study has been presented for the heat and mass transfer in non-similar bioconvection flow of nanofluid under oblique magnetic field with nonlinear radiation solar flux. In this study, second law thermodynamic analysis is also performed. Homotopy analysis method is implemented to find out the series solution of the transformed dimensionless system of nonlinear partial differential equations. The influence of leading parameters on temperature, skin friction coefficient, Nusselt number and motile microorganism flux is presented graphically. The principal findings of the present study can be summarized as follows:

- Skin friction coefficient decreases with magnetic parameter as well as bioconvection Rayleigh number whereas it increases with radiation parameter.
- Local Nusselt number is found to be a decreasing function of magnetic parameter, radiation parameter and bioconvection Rayleigh number.
- Motile microorganism flux rate is depressed with magnetic parameter and bioconvection Rayleigh number whereas it is enhanced with radiation parameter.
- Temperature of nanofluid increases with radiation parameter whereas it is decreased with Prandtl number.
- The entropy generation analysis demonstrates that the entropy generation number increases with inertial effect (Reynolds number), radiation parameter and Prandtl number whereas it decreases with increasing orientation of the magnetic field (i.e. decreasing Lorentz magnetic body force).

The present simulations provide a solid benchmark for more advanced computational simulations of solar magnetic nanofluid bioconvection fuel cell analysis and efforts in this direction, with a particular emphasis on more complex geometries (annular, pipe, cubic, etc.), are currently underway.

Author Contributions

N. Shukla (NS) initiated the project and suggested the appropriate non-similar mathematical model for present nanofluid problem. P. Rana (PR) performed the HAM analysis and developed the MAPLE codes after discussion with NS. S. Kuharat (SK) and O. Anwar Bég (OB) examined the validation of result. The manuscript was written through the contribution of all authors. All authors discussed the results, reviewed and approved the final version of the manuscript.

Conflict of Interest

The authors declared no potential conflicts of interest with respect to the research, authorship and publication of this article.

Funding

The authors received no financial support for the research, authorship and publication of this article.

References

[1] Choi, S. U. S., Eastman, J. A., Enhancing Thermal Conductivity of Fluids with Nanoparticles, Argonne National Lab., IL (United States), ANL/MSD/CP--84938; CONF-951135-29, Available: https://www.osti.gov/scitech/biblio/196525/, 2017.
[2] Buongiorno, J., Convective Transport in Nanofluids, *ASME Journal of Heat Transfer*, 128(3), 2006, 240–250.
[3] Kuznetsov, A. V., Nield, D. A., Natural Convective Boundary-Layer Flow of a Nanofluid Past a Vertical Plate: A Revised Model, *International Journal of Thermal Sciences*, 77, 2014, 126–129.
[4] Mohyud-Din, Khan, S. T., U., Hassan, S. M., Numerical Investigation of Magnetohydrodynamic Flow And Heat Transfer of Copper–Water Nanofluid

in A Channel with Non-Parallel Walls Considering Different Shapes of Nanoparticles, *Advances in Mechanical Engineering*, 8(3), 2016, 1-9.

[5] Rana, P., Bhargava, R., Bég, O. A., Numerical Solution For Mixed Convection Boundary Layer Flow Of A Nanofluid Along An Inclined Plate Embedded In A Porous Medium, *Computers & Mathematics with Applications*, 64(9), 2012, 2816–2832.

[6] Hunt, A. J., Small Particle Heat Exchangers. Department of Energy, Lawrence Berkeley Laboratory, *Energy and Environment Division*, 1978.

[7] Shehzad, S. A., Hayat, T., Alsaedi, A., Obid, M. A., Nonlinear Thermal Radiation in Three-Dimensional Flow of Jeffrey Nanofluid: A Model for Solar Energy, *Applied Mathematics and Computation*, 248, 2014, 273–286.

[8] Das, M. B., Mahata, K., Nandkeolyar, R., Mixed Convection and Nonlinear Radiation in the Stagnation Point Nanofluid flow towards a Stretching Sheet with Homogenous-Heterogeneous Reactions effects, *Procedia Engineering*, 127, 2015, 1018–1025.

[9] Uddin, M. J., Rana, P., Bég, O. A., Ismail, A. I. Md., Finite Element Simulation of Magnetohydrodynamic Convective Nanofluid Slip Flow in Porous Media with Nonlinear Radiation, *Alexandria Engineering Journal*, 55(2), 2016, 1305–1319.

[10] Khan, U., Ahmed, N., Mohyud-Din, S. T., Mohsin, B. B., Nonlinear Radiation Effects on MHD Flow of Nanofluid over A Nonlinearly Stretching/Shrinking Wedge, *Neural Computing and Application*, 28(8), 2017, 2041–2050.

[11] Ashraf, E. E., *Advected Bioconvection and the Hydrodynamics of Bounded Biflagellate Locomotion*, PhD Thesis, University of Glasgow, 2011.

[12] Das, K., Duari, P. R., Kundu, P. K., Nanofluid Bioconvection in Presence of Gyrotactic Microorganisms and Chemical Reaction in A Porous Medium, *Journal of Mechanical Science and Technology*, 29(11), 2015, 4841–4849.

[13] Kuznetsov, A. V., Avramenko, A. A., Effect of Small Particles on this Stability of Bioconvection in A Suspension of Gyrotactic Microorganisms in A Layer of Finite Depth, *International Communications in Heat and Mass Transfer*, 31(1), 2004, 1–10.

[14] Hill, N. A., Pedley, T. J., Bioconvection, *Fluid Dynamics Research*, 37(1), 2005, 1–20.

[15] Alloui, Z., Nguyen, T. H., Bilgen, E., Bioconvection of Gravitactic Microorganisms in A Vertical Cylinder, *International Communications in Heat and Mass Transfer*, 32(6), 2005, 739–747.

[16] Uddin, Md. J., Kabir, M. N., Bég, O. A., Computational Investigation of Stefan Blowing and Multiple-Slip Effects on Buoyancy-Driven Bioconvection Nanofluid Flow with Microorganisms, *International Journal of Heat and Mass Transfer*, 95, 2016, 116–130.

[17] Dhanai, R., Rana, P., Kumar, L., Lie Group Analysis for Bioconvection MHD Slip Flow and Heat Transfer of Nanofluid over An Inclined Sheet: Multiple Solutions, *Journal of the Taiwan Institute of Chemical Engineers*, 66, 2016, 283–291.

[18] Khan, W., Rashad, A., Abdou, M. M. M., Tlili, I., Natural Bioconvection Flow of A Nanofluid Containing Gyrotactic Microorganisms about A Truncated Cone, *European Journal of Mechanics - B/Fluids*, 75, 2019, 133-142.

[19] Waqas, H., Khan S. U., Hassan, M. M., Bhatti, M., Imran, M., Analysis on the Bioconvection Flow of Modified Second-Grade Nanofluid Containing Gyrotactic Microorganisms and Nanoparticles, *Journal of Molecular Liquids*, 291, 2019, 111231.

[20] Rashad, A. M., Nabwey, H. A., Gyrotactic Mixed Bioconvection Flow of A Nanofluid Past A Circular Cylinder with Convective Boundary Condition, *Journal of the Taiwan Institute of Chemical Engineers*, 99, 2019, 9–17.

[21] Khan, N. S., Shah, Q., Bhaumik, A., Kumam, P., Thounthong, P., Amiri, I., Entropy Generation in Bioconvection Nanofluid Flow Between Two Stretchable Rotating Disks, *Scientific Reports*, 10(1), 2020, 1–26.

[22] Aneja, M., Sharma, S., Kuharat, S., Beg O. A., Computation of Electroconductive Gyrotactic Bioconvection under Nonuniform Magnetic Field: Simulation of Smart Bio-Nanopolymer Coatings for Solar Energy, *International Journal of Modern of Physics*, 34(5), 2020, 2050028.

[23] Khan, S. U., Shehzad, S. A., Ali, N., Bioconvection Flow of Magnetized Williamson Nanoliquid with Motile Organisms and Variable Thermal Conductivity, *Applied Nanoscience*, 10, 2020, 3325–3336.

[24] Lu, D., Ramzan, M., Ullah, N., Chung, J. D., Farooq, U., A Numerical Treatment of Radiative Nanofluid 3D Flow Containing Gyrotactic Microorganism with Anisotropic Slip, Binary Chemical Reaction and Activation Energy, *Scientific Reports*, 7(1), 2017, 17008.

[25] Singh, P. K., Anoop, K. B., Sundararajan, T., Das, S. K., Entropy Generation Due to Flow and Heat Transfer in Nanofluids, *International Journal of Heat and Mass Transfer*, 53(21), 2010, 4757–4767.

[26] Aiboud , S., Saouli, S., Second Law Analysis of Viscoelastic Fluid over A Stretching Sheet Subject to A Transverse Magnetic Field with Heat and Mass Transfer, *Entropy*, 12(8), 2010, 1867–1884.

[27] Butt, A. S., Munawar S., Ali, A., Mehmood, A., Entropy Generation in the Blasius Flow under Thermal Radiation, *Physica Scripta*, 85(3), 2012, 035008.

[28] Bhatti, M. M., Abbas, T., Rashidi, M. M., Entropy Generation as A Practical Tool of Optimisation for Non-Newtonian Nanofluid Flow through A Permeable Stretching Surface using SLM, *Journal of Computational Design and Engineering*, 4(1), 2017, 21–28.

[29] Bég, O., Kavyani, N. Islam M., Entropy Generation in Hydromagnetic Convective Von Karman Swirling Flow: Homotopy Analysis, *International Journal of Applied Mathematics and Mechanics*, 9, 2013, 37–65.

[30] Rashidi, M. M., Parsa, A. B., Bég, O. A., Shamekhi, L., Sadri, S. M., Bég, T. A., Parametric Analysis of Entropy Generation In Magneto-Hemodynamic Flow in A Semi-Porous Channel With OHAM and DTM, *Applied Bionics and Biomechanics*, 11, 2014, 47–60.

[31] Srinivas, J., Murthy, J. V. R., Beg. O. A., Entropy Generation Analysis of Radiative Heat Transfer Effects on Channel Flow of Two Immiscible Couple Stress Fluids, *Journal of Brazilian Society of Mechanical Science and Engineering*, 39(6), 2017, 2191–2202.

[32] Akbar, N. S., Shoaib, M., Tripathi, D., Bhushan, S., Bég, O. A., Analytical Approach To Entropy Generation And Heat Transfer In CNT-Nanofluid Dynamics Through A Ciliated Porous Medium, *Journal of Hydrodynamics*, 30(2), 2018, 296–306

[33] Jangili, S., Bég, O. A., Homotopy Study of Entropy Generation in Magnetized Micropolar Flow in A Vertical Parallel Plate Channel with Buoyancy Effect, *Heat Transfer Research*, 49(6), 2018, 529–553.

[34] Ramzan, M., Mohammad, M., Howari, F., Magnetized Suspended Carbon Nanotubes Based Nanofluid Flow with Bio-Convection and Entropy Generation Past a Vertical Cone, *Scientific Reports*, 9(1), 2019, 12225.

[35] Khan, N. S., Kumam, P., Thounthong, P., Second Law Analysis with Effects of Arrhenius Activation Energy and Binary Chemical Reaction on Nanofluid Flow, *Scientific Reports*, 10(1), 2020, 1226.

[36] Buongiorno, J., et al., A Benchmark Study on the Thermal Conductivity of Nanofluids, *Journal of Applied Physics*, 106(9), 2009, 094312.

[37] Kakaç, S., Pramuanjaroenkij, A., Review of Convective Heat Transfer Enhancement with Nanofluids, *International Journal of Heat and Mass Transfer*, 52(13), 2009, 3187–3196.

[38] Wong, K. V., Leon, O. D., Applications of Nanofluids: Current and Future, *Advances in Mechanical Engineering*, 2, 2010, 519659.

[39] Mahian, O., Kianifar, A. S., Kalogirou, A., Pop, I., Wongwises, S., A Review of the Applications of Nanofluids in Solar Energy, *International Journal of Heat and Mass Transfer*, 57(2), 2013, 582–594.

[40] Sheikholeslami, M., Ganji, D. D., Nanofluid Convective Heat Transfer Using Semi Analytical and Numerical Approaches: A Review, *Journal of the Taiwan Institute of Chemical Engineers*, 65, 2016, 43–77.

[41] Myers T., Cregan, V., Ribera, H., Does Mathematics Contribute to the Nanofluid Debate?, *International Journal of Heat and Mass Transfer*, 111, 2017, 279–288.

[42] Grosan, T., Sheremet, M., Pop, I., *Heat Transfer Enhancement in Cavities Filled with Nanofluids: From Numerical to Experimental Techniques*, CRC Press, 2017.

[43] Das, S. K., Choi, S. U. S., Yu, W., Pradeep, T., *Nanofluids: Science and Technology*, Wiley, 2019.

[44] Nield, D. A., Bejan, A., *Convection in Porous Media*, New York, Springer-Verlag, 2013.

[45] Shenoy, A., Sheremet, M., Pop I., *Convective Flow and Heat Transfer from Wavy Surfaces: Viscous Fluids, Porous Media, and Nanofluids*, CRC Press 2016.

[46] Lyu, Z., Asadi, A., Alarifi, I. M., Ali, V., Foong, L. K., Thermal and Fluid Dynamics Performance of MWCNT-Water Nanofluid Based on Thermophysical Properties: An Experimental and Theoretical Study, *Scientific Reports*, 10(1), 2020, 5185.

[47] Liao, S. J., A General Approach to Get Series Solution of Non-Similarity Boundary-Layer Flows, *Communications in Nonlinear Science and Numerical Simulation*, 14(5), 2009, 2144–2159.

[48] Kousar , N., Liao, S. J., Series Solution of Non-similarity Boundary-Layer Flows Over a Porous Wedge, *Transport in Porous Media*, 83(2), 2010, 397–412.

[49] Kousar, N., Liao, S., Series Solution of Non-Similarity Natural Convection Boundary-Layer Flows Over Permeable Vertical Surface, *Science, China Physics, Mechanics and Astronomy*, 53(2), 2010, 360–368.

[50] You, X., Xu, H., Liao, S. J., On the Nonsimilarity Boundary-Layer Flows of Second-Order Fluid over a Stretching Sheet, *Journal of Applied Mechanics*, 77, 2010, 1–8.

[51] Kousar, N., Liao, S., Unsteady Non-Similarity Boundary-Layer Flows Caused by An Impulsively Stretching Flat Sheet, *Nonlinear Analysis: Real World Applications*, 12(1), 2011, 333–342.

[52] Liao, S. J., *Beyond Perturbation: Introduction to the Homotopy Analysis Method*, Chapman & Hall/CRC Press, London/Boca Ratton, 2003.

[53] Farooq, U., Zhao, Y. L., Hayat, T., Alsaedi, A., Liao, S. J., Application of the HAM-Based Mathematica Package Bvph 2.0 on MHD Falkner–Skan Flow of Nano-Fluid, *Computers & Fluids*, 111, 2015, 69–75.

[54] Bejan, A., A Study of Entropy Generatio9n in Fundamental Convective Heat Transfer, *Journal of Heat Transfer*, 101(4), 1979, 718–725.

[55] Bég, O. A., Rashidi, M. M., Bég, T. A., Asadi, M., Homotopy Analysis of Transient Magneto-Bio-Fluid Dynamics of Micropolar Squeeze Film in A Porous Medium: A Model for Magneto-Bio-Rheological Lubrication, *Journal of Mechanics in Medicine and Biology*, 12(3), 2012.

[56] Bég, T. A., Bég, O., Asadi M., Homotopy Semi-Numerical Modelling of Nanofluid Convection Boundary Layers from an Isothermal Spherical Body in a Permeable Regime, *International Journal of Microscale and Nanoscale Thermal Fluid Transport Phenomena*, 3, 2013, 237–266.

[57] Tripathi, D., Bég, O. A., Curiel-Sosa, J. L., Homotopy semi-numerical simulation of peristaltic flow of generalised Oldroyd-B fluids with slip effects, *Computer Methods in Biomechanics and Biomedical Engineering*, 17(4), 2014, 433–442.

[58] Bég, O. A., Mabood, F., Islam, M. N., Homotopy Simulation of Nonlinear Unsteady Rotating Nanofluid Flow from a Spinning Body, *International Journal of Engineering Mathematics*, 2015, 272079.

[59] Ali, N., Asghar, Z., Bég, O. A., Sajid, M., Bacterial Gliding Fluid Dynamics on A Layer of Non-Newtonian Slime: Perturbation and Numerical Study, *Journal of Theoretical Biology*, 397, 2016, 22–32.

[60] Beg, O. A., Multi-Physical Electro-Magnetic Propulsion Fluid Dynamics : Mathematical Modelling and Computation, *Mathematical Modeling : Methods, Applications and Research*, 2018, 2–88.

[61] Abdallah, I. A., Homotopy Analytical Solution of MHD Fluid Flow and Heat Transfer Problem, *Applied Mathematics & Information Sciences*, 3(2), 2017, 223–233.

[62] Hayat, T., Imtiaz, M., Alsaedi, A., Partial Slip Effects in Flow over Nonlinear Stretching Surface, *Journal of Applied Mathematics and Mechanics*, 36(11), 2015, 1513–1526.

[63] Liao, S. J., Comparison between the Homotopy Analysis Method and Homotopy Perturbation Method, *Applied Mathematics and Computation*, 169(2), 2005, 1186–1194.

[64] Gupta, V. G., Gupta, S., Application of Homotopy Analysis Method for Solving Nonlinear Cauchy Problem, *Surveys in Mathematics and its Applications*, 7, 2012, 105–116.

[65] Gorder, Van, R. A., Vajravelu, K., On The Selection Of Auxiliary Functions, Operators, And Convergence Control Parameters In The Application Of The Homotopy Analysis Method To Nonlinear Differential Equations: A General Approach, *Communications in Nonlinear Science and Numerical Simulation*, 14(12), 2009, 4078–4089

[66] Yin, X.B., Kumar, S., Kumar, D., A modified homotopy analysis method for solution of fractional wave equations, *Advances in Mechanical Engineering*, 7(12), 2015, 1–8.

[67] Wang, C. Y., Stagnation Flow towards a Shrinking Sheet, *International Journal of Non-Linear Mechanics*, 43(5), 2008, 377–382.

[68] Khan, W. A., Pop, I., Boundary-layer flow of a nanofluid past a stretching sheet, *International Journal of Heat and Mass Transfer*, 53(11), 2010, 2477–2483.

[69] Gorla, R. S. R., Sidawi, I., Free convection on a vertical stretching surface with suction and blowing, *Journal of Applied Science Research*, 52(3), 1994, 247–257.

[70] Cramer, K. R., Bai, S., Pai, S., *Magnetofluid Dynamics for Engineers and Applied Physicists*, Scripta Publishing Company, 1973.

[71] Uddin, M. J., Alginahi, Y., Bég, O. A., Kabir, M. N., Numerical Solutions for Gyrotactic Bioconvection in Nanofluid-Saturated Porous Media with Stefan Blowing and Multiple Slip Effects, *Computers & Mathematics with Applications*, 72(10), 2016, 2562–2581.

[72] Katz, E., Lioubashevski, O., Willner, I., Magnetic Field Effects on Bioelectrocatalytic Reactions of Surface-Confined Enzyme Systems: Enhanced Performance of Biofuel Cells, *Journal of American Chemical Society*, 127(11), 2005, 3979–3988

[73] Goh, W. J. et al., Iron Oxide Filled Magnetic Carbon Nanotube-Enzyme Conjugates for Recycling of Amyloglucosidase: Toward Useful Applications in Biofuel Production Process, *Langmuir*, 28, 2012, 16864–16873.

ORCID iD

Nisha Shukla https://orcid.org/0000-0002-6780-2433
Puneet Rana https://orcid.org/0000-0002-9850-763X

Publisher's Note Shahid Chamran University of Ahvaz remains neutral with regard to jurisdictional claims in published maps and institutional affiliations.